Low Perfusion Compartments in Glioblastoma Quantified by Advanced Magnetic Resonance Imaging: Correlation with Patient Survival

Chao Li, MD[1,2], Jiun-Lin Yan, MD[1,3,4], Turid Torheim, PhD[5,6], Mary A. McLean, PhD[5], Natalie R. Boonzaier, PhD[1], Yuan Huang, PhD[7,9], Bart RJ van Dijken, BSc[10], Tomasz Matys, MD PhD[7,8], Florian Markowetz, PhD[5,6], and Stephen J. Price, BSc MBBS(Hons) PhD FRCS (Neuro Surg.)[1,11]

Corresponding author: Chao Li

Mobile: +44 7732924953

Email: cl647@cam.ac.uk

FAX: +44 (0)1223 216926

[1]Brain Tumour Imaging Laboratory, Division of Neurosurgery, Department of Clinical Neuroscience, University of Cambridge, Addenbrooke's Hospital, Cambridge, UK;

[2]Department of Neurosurgery, Shanghai General Hospital, Shanghai, China;

[3]Department of Neurosurgery, Chang Gung Memorial Hospital, Keelung, Taiwan;

[4]Chang Gung University College of Medicine, Taoyuan, Taiwan;

[5]Cancer Research UK Cambridge Institute, University of Cambridge, Cambridge, UK;

[6]CRUK & EPSRC Cancer Imaging Centre in Cambridge and Manchester, Cambridge, UK;

[7]Department of Radiology, University of Cambridge, Cambridge, UK;

[8]Cancer Trials Unit Department of Oncology, Addenbrooke's Hospital, Cambridge, UK;

[9]EPSRC Centre for Mathematical and Statistical Analysis of Multimodal Clinical Imaging, University of Cambridge, Cambridge, UK;

[10]Department of Radiology, University Medical Center Groningen, University of Groningen, Groningen, the Netherlands.

[11]Wolfson Brain Imaging Centre, Department of Clinical Neuroscience, University of Cambridge, Cambridge, UK;

Running title: Low Perfusion Compartments in Glioblastoma

Funding

This study was funded by a National Institute for Health Research (NIHR) Clinician Scientist Fellowship (SJP, project reference NIHR/CS/009/011); Cambridge Trust and China Scholarship Council (CL); the Chang Gung Medical Foundation and Chang Gung Memorial Hospital, Keelung, Taiwan (JLY); CRUK & EPSRC Cancer Imaging Centre in Cambridge & Manchester (TT, grant C197/A16465); NIHR Cambridge Biomedical Research Centre (TM); the Groningen University Fund and the Marco Polo fund (BD). The views expressed are those of the author(s) and not necessarily those of the NHS, the NIHR or the Department of Health.

Conflict of Interest: none

Total word count: 7362

Abstract

Background

Glioblastoma exhibits profound intratumoral heterogeneity in blood perfusion, which may cause the inconsistent response to angiogenesis inhibitor therapy in previous clinical trials. Particularly, low perfusion may create hypoxic microenvironment in tumor and induce resistant clones. Finding validated imaging approach to define these compartments for clinical management is crucial. The aim of this study was to use physiological magnetic resonance imaging (MRI) to identify the low perfusion compartments pretherapeutically and determine their contributions to survivals.

Methods and Findings

A total of 112 newly-diagnosed supratentorial GBM patients were included in this study. Preoperative MRI included anatomical, dynamic susceptibility contrast (DSC), diffusion tensor imaging (DTI) and chemical shift imaging (CSI). All patients underwent maximal safe resection and diagnosis was confirmed by pathology. The apparent diffusion coefficient (ADC) and relative cerebral blood volume (rCBV) were calculated from DTI and DSC respectively. Using thresholding methods, two low perfusion compartments (ADC_H-$rCBV_L$ and ADC_L-$rCBV_L$) were identified with combinations of high/low ADC and low rCBV values. Metabolic analysis using CSI revealed that the two compartments displayed higher lactate and macromolecule/lipid levels than abnormal and normal controls (p = 0.017 and p<0.001, respectively), suggesting the hypoxic and pro-inflammatory microenvironment. The proportion of ADC_L-$rCBV_L$ compartment contributed to larger tumor infiltration area visualized by FLAIR (p < 0.001, r = 0.40), while the proportion of ADC_H-$rCBV_L$ contributed to smaller tumor infiltration (p = 0.001, r = -0.31). Higher lactate in the ADC_L-$rCBV_L$ compartment was associated with more invasive phenotypes visualized on diffusion tensor imaging. Survival analysis showed the volume of ADC_L-$rCBV_L$ compartment was associated with a better progression free survival (PFS) (Hazard ratio 0.490, p = 0.024) and the lactate level in this compartment contributed to a worse PFS (Hazard ratio 2.080, p = 0.049). In contrast, the lactate level in the ADC_H-$rCBV_L$ compartment contributed to a better overall survival (Hazard ratio 0.571, p = 0.024), suggesting these two compartments had different treatment response.

Conclusions

Two low perfusion compartments could be visualized by multiple advanced MRI techniques, which displayed heterogeneity in extent and intensity of hypoxia, and consequently exhibited diversity in tumor invasion and patient outcomes. Particularly, the ADC_L-$rCBV_L$ compartment may represent a treatment target which may induce resistance.

Keywords:
Glioblastoma; Magnetic Resonance Imaging; Angiogenesis; Heterogeneity.

Author Summary

Why Was This Study Done?

- Previous failure in clinical trials of angiogenesis inhibitor in glioblastoma may be caused by the inadequate understanding of angiogenesis.
- Although tumor compartments with elevated perfusion have been investigated intensively, the low perfusion compartments are yet to be studied.
- Conventional imaging approach is non-specific in revealing perfusion heterogeneity. Whether multiple modalities of quantitative MRI may help to reveal the resistant treatment target remains unclear.

What Did the Researchers Do and Find?

- We prospectively recruited 112 patients and performed multiple modality MRI scans on these patients. All the patients received maximal safe resection. After surgery, 82 patents received standard dose of chemoradiotherapy and were followed up.
- We used thresholding to identify two low perfusion compartments from preoperative MRI images and studied their volumes, metabolic profiles, contributions to tumor infiltration and patient outcomes.
- We found that two low perfusion compartments both displayed hypoxic and pro-inflammatory metabolic signatures, suggesting the selective stress in these regions. The lactate levels in these regions was associated with a larger tumor volume.

However, two compartments showed different contributions to tumor infiltration and patient outcomes.

- The ADC_L-$rCBV_L$ compartment may contribute to a larger tumor infiltration area, and the higher lactate level in this region may contribute to more invasive DTI phenotypes. The higher proportion of this compartment in tumor was associated with a better progression free survival, but the lactate level in this region was associated with a worse survival.
- The ADC_H-$rCBV_L$ compartment had a significant higher volume than the ADC_L-$rCBV_L$ compartment, and the higher lactate level in this region was associated with a better overall survival.

What Do These Findings Mean?

- The findings of this study may change the notion that the invasiveness of GBM solely stems from the highly proliferative regions and support the approach of treating GBM as a dynamic ecosystem.
- The imaging findings help to optimize the current clinical routine which is mainly based on non-specific conventional imaging. As the imaging modality used in this study has been available in clinical procedure, this approach could provide crucial information for patient personalized treatment and might be extended to other tumors.

Introduction

Glioblastoma (GBM) is a highly aggressive primary tumor in the central nervous system of adults (1). Despite of the advances in treatment, the median overall survival (OS) of GBM patients remains 14.6 months (2). Inconsistent response to treatment is a major challenge in GBM treatment stratification and could be caused by the extensive heterogeneity of this disease. Many genetically distinct cancer cell populations can exist in the same tumor and may display diverse treatment response (3, 4). Developing validated methods to explore intratumoral heterogeneity is crucial for patient subgrouping and personalized treatment.

One of the most fundamental traits of GBM is chronic angiogenesis and elevated perfusion, which has been correlated with a more invasive phenotype (5, 6). However, a potent angiogenesis inhibitor failed to demonstrate consistent benefits in clinical trials of newly diagnosed GBM (7), which suggested the current understanding of angiogenesis/perfusion might be insufficient for therapeutic targeting. Due to the aberrant microvasculature and inefficient nutrient delivery, a profound intratumor perfusion heterogeneity can be observed in GBM, and thus the blood supply and metabolism demand may be remarkably mismatched. Consequently, the sufficiently perfused subregions may hold the advantages for progression and proliferation, whereas the insufficiently perfused subregions may have a hypoxic microenvironment (8). The selective stress created thereafter is believed to have impact on clonal evolution (9), during which adaptive and resistant clones may be preferentially induced (10) . As accumulative knowledge supports the notion that tumor is a complex and dynamic ecosystem (11), there is a rising need to understand the function of low perfusion subregions and evaluate their contribution to treatment resistance.

The variation in regional perfusion may lead to the morphological heterogeneity within GBM, such as enhancement, necrosis and edema, visualized by the conventional imaging. Clinicians

commonly refer to the non-enhancing regions within contrast enhancement (CE) on post-contrast T1-weighted imaging as low perfusion regions. Intratumoral hypoxia is assessed by the extent of these regions as 'necrosis'. However, this approach has intrinsic limitations. Firstly, the enhancement observed from the weighted images depends on the time phase of acquisition (12, 13). Secondly, it is gradually realized that the contrast imaging is non-specific in addressing tumor physiology accurately, since it just reflects the leakage of blood-brain barrier.

Recently, several studies have suggested that quantitative imaging features are useful in reflecting tumor heterogeneity and identifying molecular phenotypes (11, 14-16). As such, multiparametric imaging may allow comprehensive assessment of these low perfusion compartments. The relative cerebral blood volume (rCBV) calculated from perfusion weighted imaging could potentially measure tumor vascularity (17). The apparent diffusion coefficient (ADC) estimated from diffusion imaging can potentially provide information about compartments with different cellularity/cell packing by measuring microscopic diffusivity of water molecules (13). The low perfusion regions with different metabolism demand thus may be studied from the combination of ADC and rCBV.

Due to the intratumoral heterogeneity, diverse metabolic patterns may exist in different compartments. Magnetic resonance spectroscopy (MRS) is an important *in vivo* method of assessing the intratumoral metabolic state by using the measure of proton nuclei (^{1}H) signals (18). Among these metabolites, lactate is the final product of nonoxidative glycolysis and frequently detected in hypoxic microenvironments. macromolecule and lipid levels at 0.9 ppm (ML9) detects the spectral peak of the large molecules at around 0.9 ppm, which includes proteins, lipids and nucleic acids. Recent animal studies showed that ML9 level could indicate the pro-inflammatory microglial response to immune stimulus (19). In our

study, we evaluated the hypoxic stress in the low perfusion compartments by interrogating the spectra of above two metabolites.

The heterogeneity of GBM can also be observed by its infiltrative patterns. Diffusion tensor imaging (DTI) is a sensitive method to detect the subtle white matter disruption caused by tumor infiltration (20). By decomposing the tensor into isotropic components (p) and anisotropic component (q), three imaging phenotypes of GBM (minimal, localised, and diffuse) have been identified with different invasion patterns, and have been correlated with patient outcomes and IDH mutation status, a prognostic driver mutation of gliomas (21-23).

In this exploratory study, we sought to identify the low perfusion compartments in GBM with multi-parametric MRI and understand their contributions to patient outcome. Our hypothesis is that we will identify two low perfusion compartments – one with increased cellularity (low ADC, low rCBV) that has been postulated as a population adapted to hypoxic acidic conditions (11), the other with low cellularity (high ADC, low rCBV) that will be more necrotic areas. Our aim was to quantify the impact that the relative volume of these components have on metabolic profiles and clinical outcomes.

Methods

Patient Recruitment

Patients with a radiological diagnosis of primary supratentorial GBM suitable for maximal safe surgical resection were prospectively recruited from July 2010 to April 2015. Exclusion criteria include history of previous cranial surgery or radiotherapy/chemotherapy, or who were unable to undergo MRI scanning due to non-MR compatible metallic devices. All patients had a good performance status (World Health Organization performance status 0-1). Preoperative MRI and postoperative histology were performed on all patients. All imaging

and histological data were collected prospectively. Patients were all on stable doses (8mg/day) of dexamethasone. Tumour resection was performed with the guidance of neuronavigation (StealthStation, Medtronic) and 5-aminolevulinic acid fluorescence with the maximal safe resection. Chemoradiotherapy was performed after surgery as appropriate. Extent of resection (EOR) was assessed according to the postoperative MRI scans within 72 hours as complete or partial resection of contrast enhancing tumors. All patients were followed up according to the criteria of response assessment in neuro-oncology (RANO) (24). Patient survival was analyzed for overall survival (OS) and progression free survival (PFS). The latter was often made retrospectively to avoid the issue of pseudoprogression. Patient recruitment and study design are summarized in Figure 1. This study was approved by local institutional review board. Informed written consent was obtained from all patients.

MRI acquisition

All MRI sequences were performed at a 3-Tesla MRI system (Magnetron Trio; Siemens Healthcare, Erlangen, Germany) with a standard 12-channel receive-head coil. MRI sequences were acquired as following: post-contrast T1-weighted sequence (TR/TE/TI 2300/2.98/900 ms; flip angle 9°; FOV 256 × 240 mm; 176-208 slices; no slice gap; voxel size 1.0 × 1.0 × 1.0 mm) after intravenous injection of 9 mL gadobutrol (Gadovist,1.0 mmol/mL; Bayer, Leverkusen, Germany); T2-weighted sequence (TR/TE 4840-5470/114 ms; refocusing pulse flip angle 150°; FOV 220 x 165 mm; 23-26 slices; 0.5 mm slice gap; voxel size of 0.7 x 0.7 x 5.0 mm); T2-weighted fluid attenuated inversion recovery (FLAIR) (TR/TE/TI 7840-8420/95/2500 ms; refocusing pulse flip angle 150°; FOV 250 x 200 mm; 27 slices; 1 mm slice gap; voxel size of 0.78125 x 0.78125 x 4.0 mm). DTI was acquired with a single-shot echo-planar sequence (TR/TE 8300/98 ms; flip angle 90°; FOV 192 x 192 mm; 63 slices; no slice gap; voxel size 2.0 x 2.0 x 2.0 mm). PWI was acquired with a dynamic susceptibility contrast-enhancement (DSC) sequence (TR/TE 1500/30 ms; flip angle 90°; FOV 192 x 192

mm; FOV 192 x 192 mm; 19 slices; slice gap 1.5 mm; voxel size of 2.0 x 2.0 x 5.0 mm;) with 9 mL gadobutrol (Gadovist 1.0 mmol/mL) followed by a 20 mL saline flush administered via a power injector at 5 mL/s. Multivoxel 2D ^{1}H-MRS chemical shift imaging (CSI) utilized a semi-LASER sequence (TR/TE 2000/30-35 ms; flip angle 90°; FOV 160 x 160 mm; voxel size 10 x 10 x 15-20 mm). PRESS excitation was selected to encompass a grid of 8 rows × 8 columns on T2-weighted images.

Imaging processing

For each subject, all MRI images were co-registered to T2-weighted images with an affine transformation, using the linear image registration tool (FLIRT) functions (25) in Oxford Centre for Functional MRI of the Brain (FMRIB) Software Library (FSL) v5.0.0 (Oxford, UK).(26) DSC data were processed and leakage correction was performed using NordicICE (NordicNeuroLab, Bergen, Norway). The arterial input function was automatically defined and rCBV was calculated in NordicICE. DTI images were processed with a diffusion toolbox (FDT) in FSL (27) and the isotropic component (p) and anisotropic component (q) were calculated using the previously described method (28). MRS data were processed using LCModel (Provencher, Oakville, Ontario) and the concentrations of lactate (Lac) and macromolecule and lipid levels at 0.9 ppm (ML9) were calculated as a ratio to creatine (Cr). All relevant spectra from CSI voxels of interest were assessed for artefacts using previously published criteria (29) . The values of the Cramer–Rao lower bounds were used to evaluate the quality and reliability of CSI data and values with standard deviation (SD) > 20% were discarded (29) .

Regions of interest and volumetric analysis

Tumour Regions of interest (ROIs) were manually drawn using an open-source software 3D slicer v4.6.2 (https://www.slicer.org/) (30) by a neurosurgeon with > 7 years of experience

(CL) and a researcher with > 4 years of brain tumor image analysis experience (NRB) and reviewed by a neuroradiologist with > 8 years of experience (TM) on the post-contrast T1WI and FLAIR. Inter-rater reliability testing was performed using Dice similarity coefficient scores to assure consistency among observers. For each individual patient, ROIs of normal-appearing white matter (NAWM) were drawn with the same method in the contralateral white matter as a normal control. All images were normalized by the mean value in NAWM. Further processing was done using MATLAB (The MathWorks, Inc., Natick MA). Firstly, ADC and rCBV values were obtained from each pixel within the contrast-enhancing region (CE) and pooled together as previous decribed (31). The lowest quartile of the pooled rCBV values ($rCBV_L$) were intercepted as low perfusion regions. Then the first quartile (ADC_L) and last quartile (ADC_H) of ADC map were respectively overlaid on $rCBV_L$ maps. Finally, two intersections of ADC_L-$rCBV_L$ and ADC_H-$rCBV_L$ ROIs were obtained. The pipeline of identifying two ADC-rCBV ROIs were illustrated by Figure 2. Other regions within CE outside the two ADC-rCBV ROIs were taken as abnormal controls (CE control, CEC). Raw volumes of ROIs were calculated using the function of fslmaths in FSL.(26) Proportional volumes (%) of two ADC-rCBV ROIs were calculated as the ratio of the raw volumes to CE volume.

Multivoxel MRS processing

To solve the challenge that the voxel size of MRS was greater than T2-weighted pixel, the T2-space pixels were projected to CSI space according to their coordinates using MATLAB. Thus, the metabolic status in each voxel can correspond to the pixels in the physiological maps, which have been coregistered to T2-weighted images. The proportion of T2-space tumor pixels occupying each CSI voxel was calculated. A selection rule was applied that only those CSI voxels were included when the proportion of tumor pixels were over 50%. The weight of each CSI voxel was taken as the proportion of the tumor pixels in that CSI voxel.

The summed weighted value was used as final metabolic value of the tumor ROI. This method provides an objective method for MRS voxel selection. The selection criteria for MRS data is demonstrated by Figure 3.

Statistical analysis

All analyses were performed with RStudio v3.2.3 (https://www.rstudio.com/). Continuous variables were tested with Welch Two Sample t-test. Categorical variables were tested with chi-square test or Fisher's exact test, as appropriate. Non-normal distributed variables, i.e., CSI data and tumor volume, were compared with Wilcoxon rank sum test using Benjamini-Hochberg procedure for controlling the false discovery rate in multiple comparisons. Pearson regression was used to model the relation between the volume of two ADC-rCBV ROIs and the volume of CE and FLAIR ROIs. Kaplan-Meier and Cox proportional hazards regression analyses were performed to evaluate patient survival. For the Kaplan-Meier analysis, the volumes of ROIs and MRS variables were dichotomized for OS and PFS before the log-rank test by using optimal cutoff values calculated by the function of 'surv_cutpoint' in R Package "survminer". Patients who were alive at the last known follow-up were censored. All CSI and tumor volume data were log transformed before testing in models. Significance was accepted at a two-sided significance level of alpha < 0.05.

Results

Patients and ROI volumes

A total of 131 patients were initially recruited, as demonstrated in Figure 1. After surgery, 19 (14.5%) patients were excluded due to non-GBM pathological diagnosis and 112 patients were included (mean age 59.4 years, range 22-76, 84 males). Among them, 82 (73.2%) patients received standard dose of radiotherapy plus temozolomide (TMZ) concomitant and adjuvant chemotherapy post-operatively and 79 (70.5%) patients had survival data available.

Complete resection of contrast enhanced tumor was achieved in 75 of 112 (67.0%) patients. Seven of 112 (6.3%) patients had the IDH-1 R132H mutation and 105 of 112 (93.8%) patients were IDH-1 wild type. MGMT-methylation status was available for 73 patients, among which 29 (39.7%) patients were methylated.

The interrater variability of the ROIs showed excellent agreement between the two raters. Dice scores of CE regions and FLAIR regions are 0.85 ± 0.10 and 0.86 ± 0.10 respectively. Volumetric analyses of raw and proportional ROIs were performed on 112 patients. The volume of the ADC_H-$rCBV_L$ compartment (5.7 ± 4.6 cm^3) was significantly larger than the ADC_L-$rCBV_L$ compartment (2.3 ± 2.2 cm^3) ($p < 0.001$). Two examples of ADC-rCBV compartments are shown on Figure 4 (A, D). Patients of age > 60 had larger CE volume ($p = 0.017$) and FLAIR volume ($p = 0.022$). Completely resected tumors had smaller CE volume ($p = 0.010$) and smaller ADC_H-$rCBV_L$ compartment ($p = 0.009$), suggesting a resectability bias. Patients' clinical characteristics and ROI volumes are summarized in Table 1.

Metabolic profiles of low perfusion compartments

Due to the abovementioned MRS analytic rules, lactate data were missing in 35 patients and ML9 data were missing in 23 patients. Our results showed that lactate/creatine (Lac/Cr) ratio in the ADC_H-$rCBV_L$ compartment (9.9, 95% CI 7.0-12.9) was significantly higher than in NAWM (0.08, 95% CI 0.02-0.13, $p < 0.001$) and CEC (5.0, 95% CI 4.0-6.1, $p = 0.017$). Similarly, the ADC_L-$rCBV_L$ compartment displayed higher Lac/Cr ratio (6.8, 95% CI 5.0-8.7) than NAWM ($p < 0.001$) and CEC (not significant). Both the ADC_H-$rCBV_L$ compartment (21.8, 95% CI 9.8-33.9, $p < 0.001$) and the ADC_L-$rCBV_L$ compartment (14.7, 95% CI 10.0-19.4, $p < 0.001$) showed higher ML9/Cr ratio than NAWM (0.96, 95% CI 0.83-1.09). Although not significant, the Lac/Cr and ML9/Cr ratios in the ADC_H-$rCBV_L$ compartment were higher than the ADC_L-$rCBV_L$ compartment. The Lac/Cr and ML9/Cr ratios of two

example cases are showed in Figure 4 (Lac/Cr: B, E; ML9/Cr: C, F). The Lac/Cr and ML9/Cr ratios in two compartments are compared in Figure 4 (G, H) and detailed in Table 2.

Low perfusion compartments exhibited diversity in contribution to tumor invasion

To explore the function of low perfusion compartments with tumor growth patterns, we analyzed the volumetric and metabolic characteristics of these two compartments. The results showed that CE volume was significantly correlated with the Lac/Cr ratio in the ADC_H-$rCBV_L$ compartment ($p = 0.004$, r = 0.32) and the Lac/Cr ratio in the ADC_L-$rCBV_L$ ($p < 0.001$, r = 0.42). Interestingly, the volume of tumor infiltration beyond contrast enhancement, which was delineated on FLAIR images and normalized by the CE volume, showed a moderate positive correlation with the proportional volume of the ADC_L-$rCBV_L$ compartment ($p < 0.001$, r = 0.40) and negative correlation with the proportional volume of the ADC_H-$rCBV_L$ compartment ($p = 0.001$, r = -0.31). The above correlations are demonstrated in Figure 5.

To further explore the relation between hypoxia and tumor invasiveness, we investigated the invasive phenotypes (Figure 6) of 64 patients overlapping with a previously reported cohort (22). The volume of the two compartments did not show significant difference among the three groups. However, in the ADC_L-$rCBV_L$ compartment, the minimally invasive phenotype displayed significantly lower Lac/Cr ratio than the localised phenotype ($p = 0.008$) and diffuse phenotype ($p = 0.044$). No significant difference was found with the ADC_H-$rCBV_L$ compartment. The invasive phenotypes and the Lac/Cr ratios in ROIs are detailed in Table 3.

Low perfusion compartments exhibited diversity in contribution to treatment response

We analyzed the available survival data of 79 patients, who received maximal surgery followed by standard regimen of radiotherapy with concomitant temozolomide (TMZ)

chemotherapy followed by adjuvant TMZ chemotherapy. The median PFS and OS of these patients were 262 days (range 25-1130 days) and 424 days (range 52-1376 days) respectively.

Due to the criteria of MRS voxel selection, the sample size of MRS data was smaller than other factors. To test the contribution of the intensity of hypoxia (measured by Lac/Cr ratio) to patient survival, we firstly used univariate models to select the most significant factors and put those factors together with the Lac/Cr ratios into the multivariate model. In univariate modelling of PFS, EOR (HR = 2.821, p = 0.001), MGMT-methylation status (HR = 0.364, p = 0.007) and the volume of ADC_L-$rCBV_L$ compartment (HR = 0.723, p = 0.019) significantly contributed to PFS. In multivariate modelling of PFS, EOR (HR = 3.868, p = 0.044), MGMT-methylation status (HR =0.247, p = 0.013), the proportional volume of ADC_L-$rCBV_L$ compartment (HR = 0.454, p = 0.013) and the Lac/Cr ratio in the ADC_L-$rCBV_L$ compartment (HR = 2.598, p = 0.012) significantly contributed to PFS.

In univariate modelling of OS, EOR (HR =2.040, p = 0.018), and the volume of CE (HR =1.018, $p < 0.001$) significantly contributed to OS. In multivariate modelling of OS, EOR (HR =3.923, p = 0.011), the volume of CE (HR =1.024, p = 0.021) and the Lac/Cr ratio in the ADC_H-$rCBV_L$ compartment (HR = 0.571, p = 0.024) significantly contributed to OS. The results of the Cox proportional hazards models are described in Table 4. The survival curve using Kaplan-Meier method with Log-rank test are demonstrated in Figure 7.

Discussion

We hypothesized that biologically distinct tumor compartments may exhibit divergent imaging properties, which could be captured by multiple physiological sequences; and thus compensate the non-specificity of contrast enhanced T1 imaging. Hence, we used multiple scale and spatial mapping of physiological sequences to delineate the regional variations of

tumor compartments. Indeed, we uncovered two low perfusion compartments which displayed diverse metabolic profiling and distinct prognostic values.

The clinical values of physiological biomarkers we used have been extensively assessed previously. Among them, rCBV is associated with tumor angiogenesis and proliferation. A recent study found rCBV could indicate IDH mutation status, which was associated with hypoxia-initiated angiogenesis (32). Consistent with above findings, our results provided evidence for the value of rCBV in assessing hypoxia-related angiogenesis. We used another marker, ADC to reflect the structural compartments by detecting the movement of water molecules. Decreased ADC is thought to represent higher tumor cellularity/cell packing and associated with shorter survival (33). A previous study showed that different ADC characteristics could indicate molecular subtypes (34). In our study, we did find the two compartments identified by different ADC scales were distinct in volume, location and invasiveness, which proved the value of ADC in depicting tumor biological changes.

As quantitative imaging is realized to be mineable data in hypothesis testing, previous studies used an ecologic method to reveal the multiple habitats within tumor, which may represent the distribution pattern of various adaptive phenotypes under selective pressure (11). The imaging heterogeneity revealed by these habitats may effectively predict patient survival (35). Consistent with above studies, our current study showed this approach could visualize two low perfusion compartments with higher lactate levels than normal and abnormal controls, which indicated the hypoxic stress existing in these two compartments. However, with similar perfusion levels in these two compartments, the higher cellularity (ADC_L) in the ADC_L-$rCBV_L$ compartment suggest that this compartment may display higher degree of mismatched perfusion and metabolism demand. Coincidently, the nonlinear relation between ADC and lactate revealed in our results might also correspond to a recent work by Gadda et

al, which suggested the association between ADC and lactate in HGG may be compartment-restricted (36). The elevated ML9/Cr ratios of these two compartments in our results may suggest these two compartments displayed elevated inflammation response. This finding corresponds to previous results showing that necrotic cells may recruit tumor-promoting inflammatory cells (37, 38).

The constant change in tumor microenvironment may lead to the dynamics of clonal evolution. The vicious cycle of proliferation, hypoxia, angiogenesis and migration presumably drives the tumor expansion and invasion (10). This hypothesis may be supported by the positive correlation between the Lac/Cr ratios in the two compartments with CE tumor volume in our results. However, only the proportional volume of the ADC_L-$rCBV_L$ compartment was correlated with the non-enhancing regions beyond CE, suggesting they might be more responsible for tumor infiltration. This might also be supported by our findings that minimally invasive phenotypes displayed significantly lower lactate levels in the ADC_L-$rCBV_L$ compartment.

It is thought that adaptable clones from low perfusion regions may lead to tumor recurrence and worse patient survival. To test this hypothesis, we investigate the contributions of the two compartments to patient survivals in a cohort who have received standard dose of CCRT. Interestingly, the Lac/Cr ratio in the two compartments had distinct contributions to patient outcomes (ADC_H-$rCBV_L$: HR 0.571; ADC_L-$rCBV_L$: HR 2.080), suggesting that the resistant phenotypes induced by hypoxia might mainly nest in the ADC_L-$rCBV_L$ compartment. Additionally, we found that the volume of ADC_L-$rCBV_L$ compartment significantly contributed to a better PFS in the multivariate model, while the Lac/Cr ratio significantly contributed to a worse PFS in the multivariate model. These results suggested that the extent of low perfusion (indicated by the volume) and intensity of hypoxia (indicated by the lactate

level) have different clinical implications. Specifically, the higher proportion of the ADC_L-$rCBV_L$ compartment may represent a relatively lower proliferative phenotype, while the more intensive hypoxia in this compartment may represent a more aggressive phenotype.

Our findings have clinical significance. Recently, an evolutionary life history approach was proposed, which suggested that the treatment focus should be put on the selective pressure within tumor (39). Since radiotherapy and chemotherapy may cause selective stress, our findings of possibly resistant target regions might give us insight for the selection of above approach. Additionally, it is postulated that antiangiogenic agents failed to demonstrate consistent response because it can induce the adaptive clones and thus cause treatment resistance (40-42). Our findings of the two low perfusion compartments may provide indications for selection of antiangiogenic therapy. Particularly, we suggest more attention might be needed for patients with larger volumes of ADC_L-$rCBV_L$ compartment when considering antiangiogenic agents. The possibility of aggravating hypoxia in this compartment may lead to a more aggressive phenotype.

There are some limitations in our study. Firstly, it is a single cohort study without an independent validation cohort. Secondly, we did not optimize the cut-off values defining the two compartments, but rather chose to use the upper and lower quartiles of the rCBV and ADC. As the ^{1}H-MRS voxels were larger than T2 space voxels, we had fewer patients with lactate data available and the multivariate analysis was done with a smaller sample size. Lastly, although our imaging markers are well validated histologically from other studies, biological validation based on multiple sampling might be needed for further testing of the ecology theory.

In conclusion, our results showed that two low perfusion compartments could be visualized by multiple advanced tumor imaging. These compartments displayed heterogeneity in extent and intensity of hypoxia, and consequently exhibited diversity in tumor invasion and treatment response. The possible solution of *in vivo* measurement of these compartments advanced by multi-parametric MRI techniques shows potential in personalized treatment strategy and response determination.

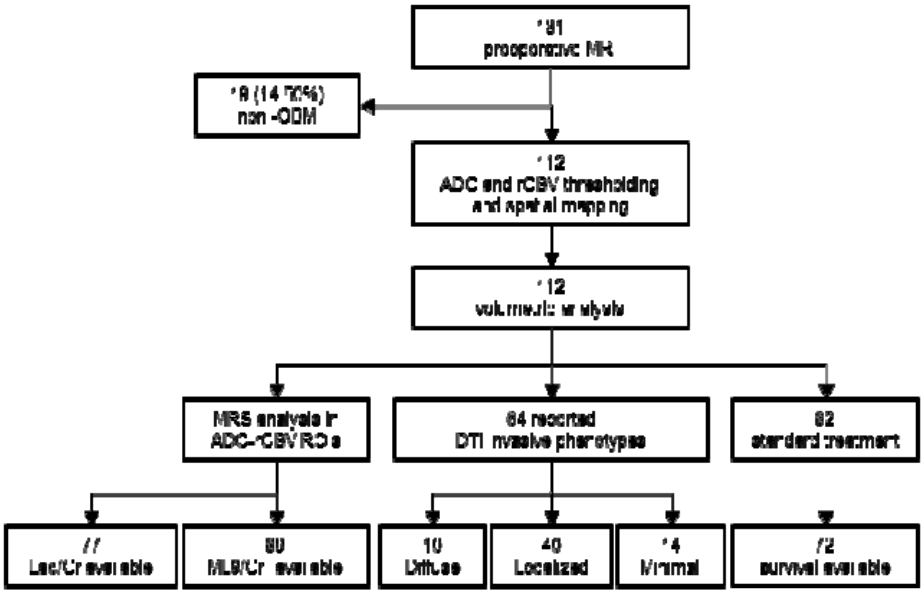

Figure 1. Flow diagram of study design and patient recruitment. Nineteen patients were excluded due to pathological non-GBM diagnosis. Due to the criteria of multiple voxel selection, patients with missing Lac/Cr and ML9/Cr data were excluded in MRS analysis. DTI invasive phenotypes were correlated with the 64 patients overlapping with a previously reported cohort. Patient survival was reviewed retrospectively to exclude psuedoprogression and was only analyzed in those who received standard chemoradiotherapy.

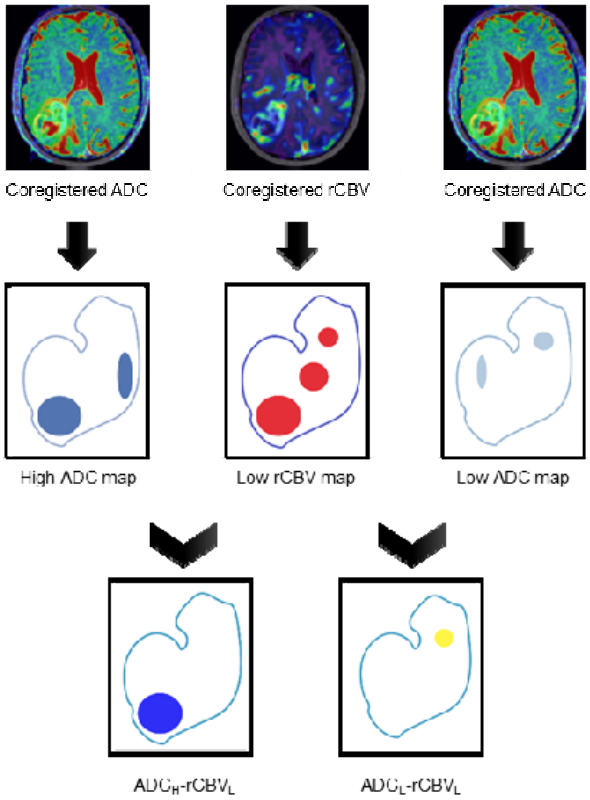

Figure 2. Illustration of the pipeline to identify two ADC-rCBV compartments. Both ADC and rCBV maps were coregistered to T2 space and tumor regions were segmented manually. Low perfusion tumor region was partitioned using a thresholding method. With the same method, two ADC subregions were partitioned using high and low thresholds respectively. The intersection of low rCBV maps and two ADC maps were obtained with a spatial mapping method.

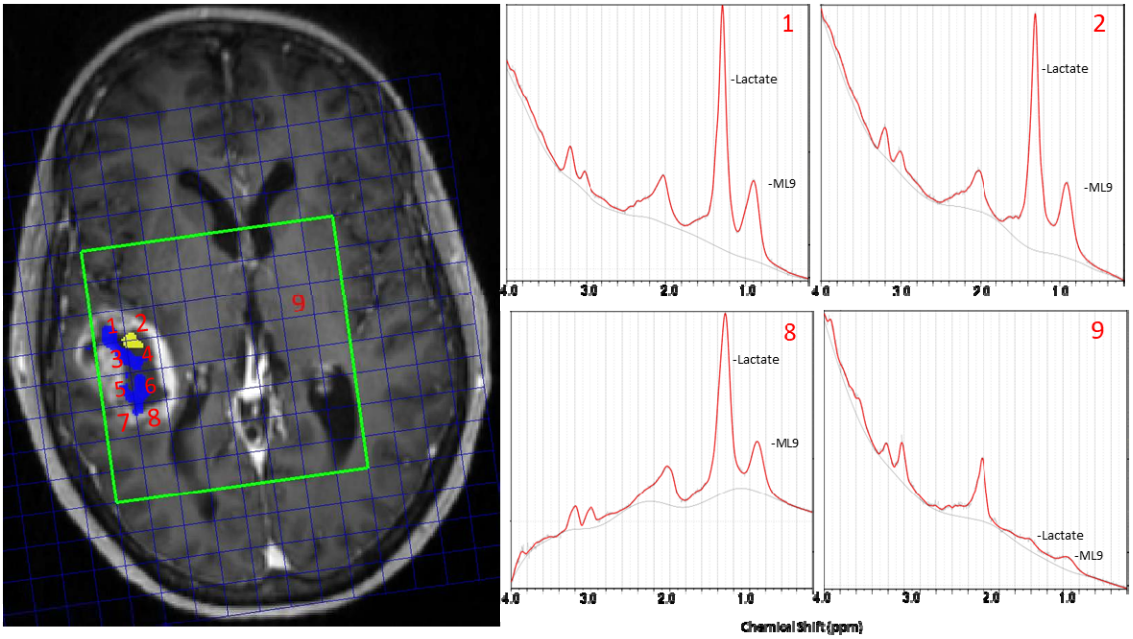

Figure 3. Illustration of multiple voxel MRS analysis. Left: the selection criteria. The T2-space pixels were projected to CSI space according to their coordinates. The proportion of T2-space tumor pixels occupying each CSI voxel was calculated. A criteria was applied that only those CSI voxels were included when the proportion of tumor voxels are over 50%. In this case, grid 1-8 met the criteria. A weighted average metabolite content for each region was calculated from the metabolite content of each voxel within it weighted by that voxel's percentage tumour content (ADC_L-$rCBV_L$ [yellow], grid 1-4 were counted; ADC_H-$rCBV_L$ [blue]: grid 1 and 3-6 were counted; abnormal control [CEC]: grid 1-8 were counted). Right: Example spectra of ROIs. Each spectrum corresponds to the grids on the left. Grid 1: lactate/Cr ratio 11.9, ML9/Cr ratio: 12.1; grid 2: lactate/Cr ratio 4.9, ML9/Cr ratio: 10.9; grid 8: lactate/Cr ratio 1.5, ML9/Cr ratio: 5.4; grid 9 (NAWM): lactate/Cr ratio 0, ML9:1.6.

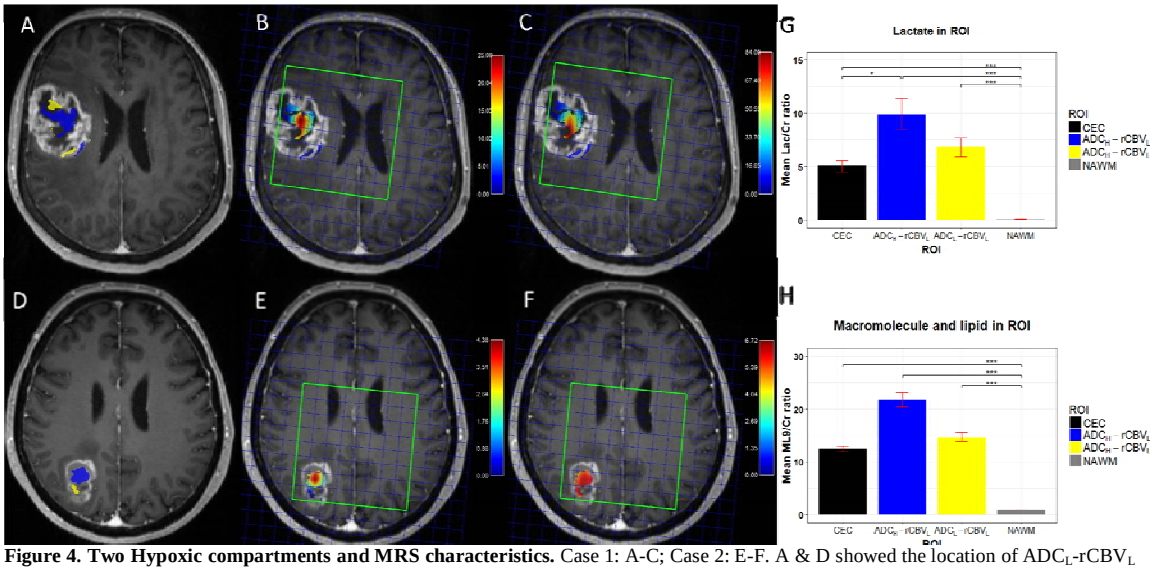

Figure 4. Two Hypoxic compartments and MRS characteristics. Case 1: A-C; Case 2: E-F. A & D showed the location of ADC_L-$rCBV_L$ (yellow) and ADC_H-$rCBV_L$ (blue) compartments. B & E demonstrated the Lac/Cr ratios of the two compartments. C & F demonstrated the ML9/Cr ratios in two compartments. The color bar showed the level of metabolites (red: high, blue: low). Note that case 1 showed greater tumor volume and higher lactate level. G & H demonstrated the MRS characteristics of the compartments. Yellow: ADC_L-$rCBV_L$; blue: ADC_H-$rCBV_L$; black: contrast-enhancing control (CEC); grey: normal-appearing white matter (NAWM). G: mean Lac/Cr level; H: mean ML9/Cr. *: $p < 0.05$; **: $p < 0.01$; ***: $p < 0.001$.

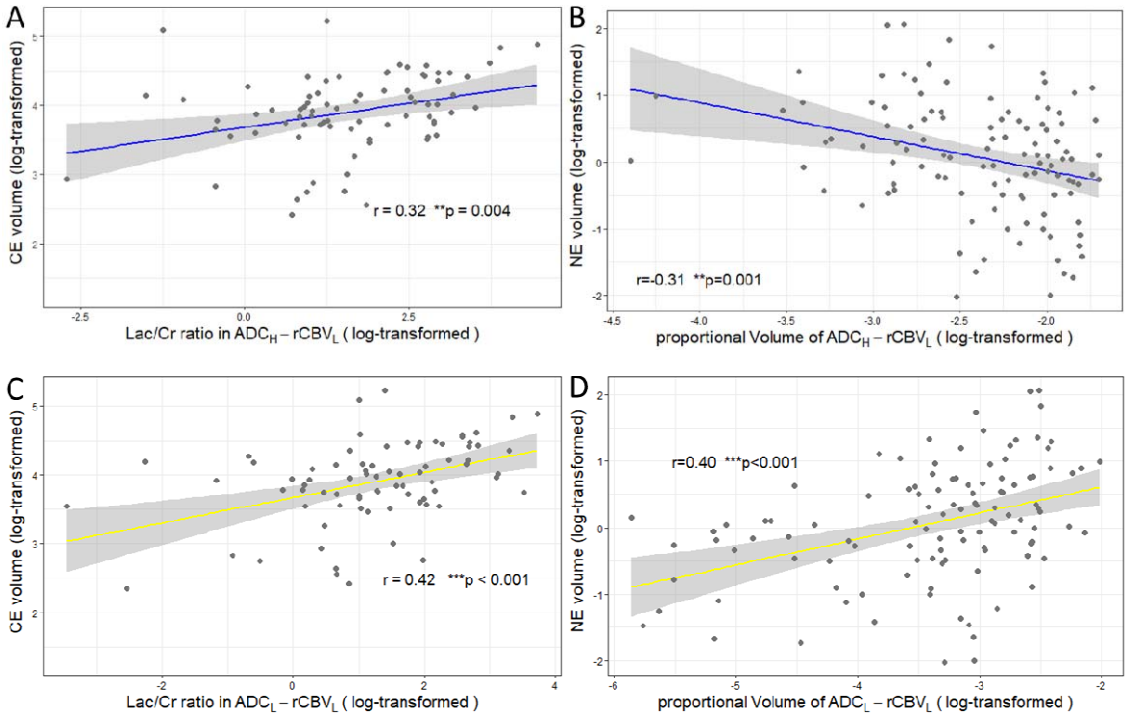

Figure 5. Correlations between two compartments with contrast enhanced tumor and tumor infiltration. (A), Contrast-enhanced (CE) volume was significantly correlated with the Lac/Cr ratio in the ADC$_H$-rCBV$_L$ compartment, and (C), the Lac/Cr ratio in the ADC$_L$-rCBV$_L$. (B), non-enhancing (NE) tumor (measured by the volume of FLAIR beyond contrast enhancement) showed a moderate positive correlation with the proportional volume (log-transformed) of the ADC$_L$-rCBV$_L$ compartment and (D), negative correlation with the proportional volume (log-transformed) of the ADC$_H$-rCBV$_L$ compartment. *: $p < 0.05$; **: $p < 0.01$; ***: $p < 0.001$.

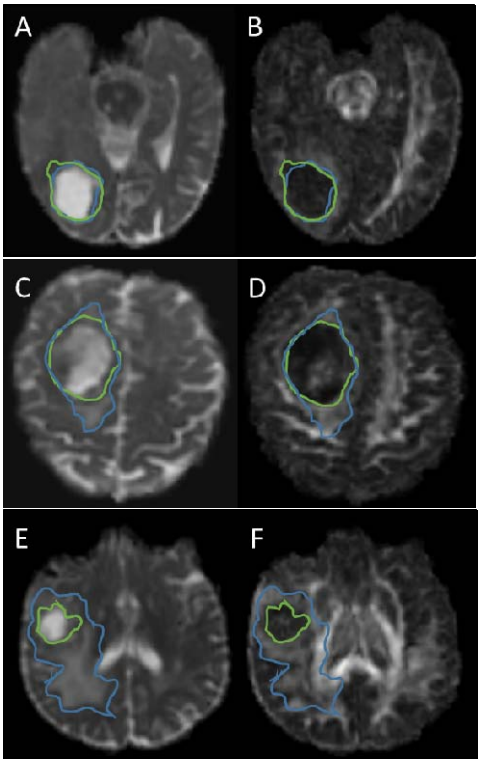

Figure 6. Examples of DTI invasive phenotypes. (A), (C), (E): DTI-p maps, abnormality outlined by the blue line; (B), (D), (F): DTI-q maps, abnormality outlined by the green line. (A) & (B) show a minimal invasive phenotype. The isotropic abnormality is similar with the anisotropic abnormality. (C) & (D) show a localised invasive phenotype. The isotropic abnormality is larger than the anisotropic abnormality in one direction. (E) & (F) show a diffuse invasive phenotype. The isotropic abnormality is larger than the anisotropic abnormality in more than one direction.

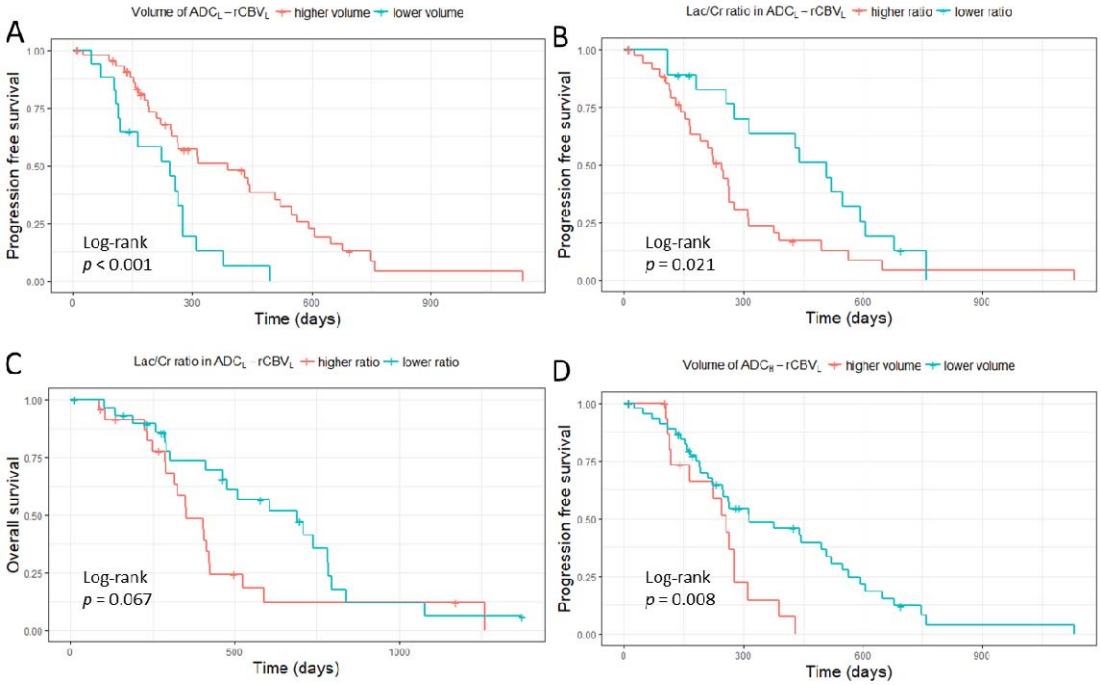

Figure 7. Kaplan-Meier plots of survival analysis. Log-rank test showed larger proportional volume of ADC_L-$rCBV_L$ compartment was associated with better PFS ($p < 0.001$) (A), while higher Lac/Cr ratio in this compartment was associated with a worse PFS (p =0.021) (B) and marginally asscociated with OS (p = 0.067) (C). Larger proportional volume of ADC_H-$rCBV_L$ compartment was associated with worse PFS (p =0.008) (D).

Table 1. Patient clinical characteristics and ROI volumes

Variable	Patient number	CE		FLAIR		ADC_H-$rCBV_L$		ADC_L-$rCBV_L$	
		Mean ± SD (cm^3)	*p*	Mean ± SD (cm^3)	*p*	Mean ± SD (cm^3)	*p*	Mean ± SD (cm^3)	*p*
Age at diagnosis									
<60	38	41.9±24.0	**0.017**	101.4±55.4	0.243	4.3±3.7	**0.022**	1.9±1.6	0.185
≥60	74	58.6±35.7		119.5±63.8		6.3±4.8		2.5±2.4	
Sex									
Male	84	54.5±34.1	0.506	115.2±62.8	0.703	5.8±4.6	0.750	2.4±2.3	0.369
Female	28	48.5±30.0		107.7±57.8		5.4±4.5		1.9±1.8	
Extent of resection									
Complete	75	45.8±26.0	**0.010**	106.0±58.0	0.087	4.8±3.9	**0.009**	2.1±1.8	0.532
Partial	37	67.4±40.8		128.3±66.1		7.5±5.2		2.6±2.8	
MGMT-methylation status*									
Methylated	29	51.3±34.8	0.512	111.8±74.3	0.314	5.3±4.3	0.320	2.1±2.7	0.315
Unmethylated	44	55.4±29.3		122.7±60.1		6.3±4.3		2.2±1.9	
IDH-1 mutation status									
Mutant	7	54.6±35.4	0.901	102.2±69.1	0.638	5.8±4.9	0.741	2.2±1.7	0.857
Wild-type	105	52.9±33.1		114.1±61.1		5.6±4.6		2.3±2.2	

*MGMT-methylation status unavailable for 39 patients; mean ± SD of original data. CE : Contrast-enhancing; cm: centimeters; FLAIR : fluid attenuated inversion recovery; ADC_L-$rCBV_L$: region of low-ADC and low-rCBV; ADC_H-$rCBV_L$: region of high-ADC and low-rCBV; IDH-1: Isocitrate dehydrogenase1; MGMT: O-6-methylguanine-DNA methyltransferase; SD: Standard deviation.

Table 2. Metabolic statistics

Lac/Cr					
	Descriptive		ADC_L-$rCBV_L$	CEC-ROI	NAWM-ROI
ROI	Mean ± SD	95% CI	*p*	*p*	*p*
ADC_H-$rCBV_L$	9.9±13.0	7.0-12.9	0.158	**0.017**	< **0.001**
ADC_L-$rCBV_L$	6.8±8.0	5.0-8.7	/	0.384	< **0.001**
CEC	5.0±4.8	4.0-6.1	/	/	< **0.001**
NAWM	0.08±0.25	0.02-0.13	/	/	/
ML9/Cr					
	Descriptive		ADC_L-$rCBV_L$	CEC-ROI	NAWM-ROI
ROI	Mean ± SD	95% CI	*p*	*p*	*p*
ADC_H-$rCBV_L$	21.8±57.4	9.8-33.9	0.10	0.10	< **0.001**
ADC_L-$rCBV_L$	14.7±22.4	10.0-19.4	/	0.85	< **0.001**
CEC	12.5±19.5	8.4-16.6	/	/	< **0.001**
NAWM	0.96±0.63	0.83-1.1	/	/	/

ROI: region of interest; ADC_L-$rCBV_L$: ROI of low-ADC and low-rCBV; ADC_H-$rCBV_L$: ROI of high-ADC and low-rCBV; CEC: contrast enhancement control; NAWM: normal appearing white matter; Lac: lactate; ML9: Macromolecule and lipid at 0.9ppm; Cr: creatine; CI: confidence interval.

Table 3. Invasive phenotypes

		Diffuse	Localised	Minimal	Comparisons		
		10 (15.6%)	40 (62.5%)	14 (21.9%)	Localised -Diffuse	Minimal-Diffuse	Minimal-Localised
ROI	Variable	Mean ± SD	Mean ± SD	Mean ± SD	*p*	*p*	*p*
CE	Volume (cm^3) *	53.8±35.0	39.7±16.0	52.7±36.2	0.660	0.988	0.856
FLAIR	Volume (cm^3) *	116.7±57.3	82.0±31.5	85.2±68.4	0.225	0.070	0.781
ADC_H-$rCBV_L$	Volume #	0.10±0.04	0.08±0.03	0.12±0.04	0.139	0.457	0.083
ADC_L-$rCBV_L$	Volume #	0.04±0.03	0.06±0.03	0.03±0.02	0.542	0.189	0.062
ADC_H-$rCBV_L$	Lac/Cr	10.7±16.9	11.1±10.4	13.3±19.1	0.791	0.901	0.999
ADC_L-$rCBV_L$	Lac/Cr	7.1±10.2	8.2±5.9	3.5±6.4	0.342	**0.044**	**0.008**
CEC	Lac/Cr	4.8±4.7	5.0±3.1	5.2±8.7	0.678	0.467	0.243

*Raw volumes; #Proportional volumes; ROI: region of interest; CE: contrast enhancement; cm: centimeters; FLAIR: fluid attenuated inversion recovery; ADC_L-$rCBV_L$: ROI of low-ADC and low-rCBV; ADC_H-$rCBV_L$: ROI of high-ADC and low-rCBV; CEC: contrast enhancement control; Lac: lactate; Cr : creatine ; SD: Standard déviation.

Table 4. Univariate and multivariate modeling of survivals

Factor	PFS						OS					
	Univariate			Multivariate			Univariate			Multivariate		
	HR	95%CI	p	HR	95%CI	p	HR	95%CI	p	HR	95%CI	p
Age	1.004	0.979-1.029	0.758				1.000	0.974 -1.027	0.988			
Sex (M)	1.555	0.923-2.618	**0.097**	1.185	0.489-2.868	0.707	1.243	0.695-2.222	0.464			
EOR	2.821	1.556-5.114	**0.001**	3.005	0.847-10.67	0.089	2.040	1.132-3.676	**0.018**	3.923	1.367-11.26	**0.011**
MGMT methylation status*	0.364	0.175- 0.756	**0.007**	0.235	0.077-0.713	**0.011**	0.524	0.266-1.032	**0.062**	0.380	0.125-1.160	0.089
IDH mutation status	0.986	0.356-2.733	0.978				1.038	0.369-2.926	0.943			
CE volume[#]	1.005	0.996-1.015	0.297				1.018	1.008-1.029	**<0.001**	1.024	1.004-1.045	**0.021**
Flair volume[#]	0.999	0.995-1.003	0.694				1.001	0.997-1.006	0.518			
ADC_L-$rCBV_L$ volume[†]	0.723	0.552-0.947	**0.019**	0.490	0.263-0.912	**0.024**	0.823	0.613-1.106	0.196			
ADC_H-$rCBV_L$ volume[†]	1.105	0.661-1.848	0.703				0.827	0.459-1.489	0.527			
Lac/Cr in ADC_H-$rCBV_L$				0.881	0.537-1.444	0.615				0.571	0.352-0.927	**0.024**
Lac/Cr in ADC_L-$rCBV_L$				2.080	1.003-4.313	**0.049**				1.838	0.892-3.787	0.099
Lac/Cr in CEC				0.534	0.234-1.218	0.136				0.749	0.301-1.864	0.535

*MGMT-methylation status unavailable for 29 patients; [#]Raw volumes; [†]Log-transformed proportional volumes; PFS: progression free survival; OS: overall survival; HR: hazard ratio; CI: confidence interval; IDH-1: Isocitrate dehydrogenase1; MGMT: O-6-methylguanine-DNA methyltransferase; CE: Contrast-enhancing; FLAIR: fluid attenuated inversion recovery; Lac: lactate; ADC_L-$rCBV_L$: region of low-ADC and low-rCBV; ADC_H-$rCBV_L$: region of high-ADC and low-rCBV; CEC: contrast enhanced control.

1. Weller M, van den Bent M, Tonn JC, Stupp R, Preusser M, Cohen-Jonathan-Moyal E, et al. European Association for Neuro-Oncology (EANO) guideline on the diagnosis and treatment of adult astrocytic and oligodendroglial gliomas. Lancet Oncol. 2017.
2. Stupp R, Mason WP, van den Bent MJ, Weller M, Fisher B, Taphoorn MJ, et al. Radiotherapy plus concomitant and adjuvant temozolomide for glioblastoma. N Engl J Med. 2005;352(10):987-96.
3. Verhaak RG, Hoadley KA, Purdom E, Wang V, Qi Y, Wilkerson MD, et al. Integrated genomic analysis identifies clinically relevant subtypes of glioblastoma characterized by abnormalities in PDGFRA, IDH1, EGFR, and NF1. Cancer Cell. 2010;17(1):98-110.
4. Sottoriva A, Spiteri I, Piccirillo SG, Touloumis A, Collins VP, Marioni JC, et al. Intratumor heterogeneity in human glioblastoma reflects cancer evolutionary dynamics. Proc Natl Acad Sci U S A. 2013;110(10):4009-14.
5. Hanahan D, Weinberg RA. Hallmarks of cancer: the next generation. Cell. 2011;144(5):646-74.
6. Lathia JD, Heddleston JM, Venere M, Rich JN. Deadly teamwork: neural cancer stem cells and the tumor microenvironment. Cell Stem Cell. 2011;8(5):482-5.
7. Chinot OL, Wick W, Mason W, Henriksson R, Saran F, Nishikawa R, et al. Bevacizumab plus Radiotherapy-Temozolomide for Newly Diagnosed Glioblastoma. New Engl J Med. 2014;370(8):709-22.
8. Gillies RJ, Schornack PA, Secomb TW, Raghunand N. Causes and effects of heterogeneous perfusion in tumors. Neoplasia. 1999;1(3):197-207.
9. Quail DF, Joyce JA. Microenvironmental regulation of tumor progression and metastasis. Nat Med. 2013;19(11):1423-37.
10. Pistollato F, Abbadi S, Rampazzo E, Persano L, Della Puppa A, Frasson C, et al. Intratumoral Hypoxic Gradient Drives Stem Cells Distribution and MGMT Expression in Glioblastoma. Stem Cells. 2010;28(5):851-62.
11. Gatenby RA, Grove O, Gillies RJ. Quantitative imaging in cancer evolution and ecology. Radiology. 2013;269(1):8-15.
12. O'Connor JPB, Rose CJ, Waterton JC, Carano RAD, Parker GJM, Jackson A. Imaging Intratumor Heterogeneity: Role in Therapy Response, Resistance, and Clinical Outcome. Clin Cancer Res. 2015;21(2):249-57.
13. O'Connor JPB, Jackson A, Asselin MC, Buckley DL, Parker GJM, Jayson GC. Quantitative imaging biomarkers in the clinical development of targeted therapeutics: current and future perspectives. Lancet Oncol. 2008;9(8):766-76.
14. Zhou M, Hall L, Goldgof D, Russo R, Balagurunathan Y, Gillies R, et al. Radiologically Defined Ecological Dynamics and Clinical Outcomes in Glioblastoma Multiforme: Preliminary Results. Transl Oncol. 2014;7(1):5-13.
15. Itakura H, Achrol AS, Mitchell LA, Loya JJ, Liu T, Westbroek EM, et al. Magnetic resonance image features identify glioblastoma phenotypic subtypes with distinct molecular pathway activities. Sci Transl Med. 2015;7(303):303ra138.
16. Aerts HJWL, Velazquez ER, Leijenaar RTH, Parmar C, Grossmann P, Cavalho S, et al. Decoding tumour phenotype by noninvasive imaging using a quantitative radiomics approach. Nat Commun. 2014;5.
17. Law M, Young RJ, Babb JS, Peccerelli N, Chheang S, Gruber ML, et al. Gliomas: Predicting time to progression or survival with cerebral blood volume measurements at dynamic susceptibility-weighted contrast-enhanced perfusion MR imaging. Radiology. 2008;247(2):490-8.
18. Padhani AR, Miles KA. Multiparametric Imaging of Tumor Response to Therapy. Radiology. 2010;256(2):348-64.

19. Pardon MC, Yanez Lopez M, Yuchun D, Marjanska M, Prior M, Brignell C, et al. Magnetic Resonance Spectroscopy discriminates the response to microglial stimulation of wild type and Alzheimer's disease models. Sci Rep. 2016;6:19880.
20. Price SJ, Jena R, Burnet NG, Hutchinson PJ, Dean AF, Pena A, et al. Improved delineation of glioma margins and regions of infiltration with the use of diffusion tensor imaging: An image-guided biopsy study. Am J Neuroradiol. 2006;27(9):1969-74.
21. Price SJ, Jena R, Burnet NG, Carpenter TA, Pickard JD, Gillard JH. Predicting patterns of glioma recurrence using diffusion tensor imaging. Eur Radiol. 2007;17(7):1675-84.
22. Price SJ, Allinson K, Liu H, Boonzaier NR, Yan JL, Lupson VC, et al. Less Invasive Phenotype Found in Isocitrate Dehydrogenase-mutated Glioblastomas than in Isocitrate Dehydrogenase Wild-Type Glioblastomas: A Diffusion-Tensor Imaging Study. Radiology. 2017;283(1):215-21.
23. Beiko J, Suki D, Hess KR, Fox BD, Cheung V, Cabral M, et al. IDH1 mutant malignant astrocytomas are more amenable to surgical resection and have a survival benefit associated with maximal surgical resection. Neuro-Oncology. 2014;16(1):81-91.
24. Wen PY, Macdonald DR, Reardon DA, Cloughesy TF, Sorensen AG, Galanis E, et al. Updated response assessment criteria for high-grade gliomas: response assessment in neuro-oncology working group. J Clin Oncol. 2010;28(11):1963-72.
25. Jenkinson M, Bannister P, Brady M, Smith S. Improved optimization for the robust and accurate linear registration and motion correction of brain images. Neuroimage. 2002;17(2):825-41.
26. Smith SM, Jenkinson M, Woolrich MW, Beckmann CF, Behrens TEJ, Johansen-Berg H, et al. Advances in functional and structural MR image analysis and implementation as FSL. Neuroimage. 2004;23:S208-S19.
27. Behrens TEJ, Woolrich MW, Jenkinson M, Johansen-Berg H, Nunes RG, Clare S, et al. Characterization and propagation of uncertainty in diffusion-weighted MR imaging. Magnet Reson Med. 2003;50(5):1077-88.
28. Pena A, Green HAL, Carpenter TA, Price SJ, Pickard JD, Gillard JH. Enhanced visualization and quantification of magnetic resonance diffusion tensor imaging using the p : q tensor decomposition. Brit J Radiol. 2006;79(938):101-9.
29. Price SJ, Young AMH, Scotton WJ, Ching J, Mohsen LA, Boonzaier NR, et al. Multimodal MRI Can Identify Perfusion and Metabolic Changes in the Invasive Margin of Glioblastomas. J Magn Reson Imaging. 2016;43(2):487-94.
30. Fedorov A, Beichel R, Kalpathy-Cramer J, Finet J, Fillion-Robin JC, Pujol S, et al. 3D Slicer as an image computing platform for the Quantitative Imaging Network. Magn Reson Imaging. 2012;30(9):1323-41.
31. Boonzaier NR, Larkin TJ, Matys T, van der Hoorn A, Yan JL, Price SJ. Multiparametric MR Imaging of Diffusion and Perfusion in Contrast-enhancing and Nonenhancing Components in Patients with Glioblastoma. Radiology. 2017:160150.
32. Kickingereder P, Sahm F, Radbruch A, Wick W, Heiland S, von Deimling A, et al. IDH mutation status is associated with a distinct hypoxia/angiogenesis transcriptome signature which is non-invasively predictable with rCBV imaging in human glioma. Sci Rep-Uk. 2015;5.
33. Shiroishi MS, Boxerman JL, Pope WB. Physiologic MRI for assessment of response to therapy and prognosis in glioblastoma. Neuro Oncol. 2016;18(4):467-78.
34. Ellingson BM. Radiogenomics and Imaging Phenotypes in Glioblastoma: Novel Observations and Correlation with Molecular Characteristics. Curr Neurol Neurosci. 2015;15(1).

35. Zhou M, Chaudhury B, Hall LO, Goldgof DB, Gillies RJ, Gatenby RA. Identifying spatial imaging biomarkers of glioblastoma multiforme for survival group prediction. J Magn Reson Imaging. 2016.
36. Gadda D, Mazzoni LN, Pasquini L, Busoni S, Simonelli P, Giordano GP. Relationship between Apparent Diffusion Coefficients and MR Spectroscopy Findings in High-Grade Gliomas. J Neuroimaging. 2017;27(1):128-34.
37. Gocheva V, Wang HW, Gadea BB, Shree T, Hunter KE, Garfall AL, et al. IL-4 induces cathepsin protease activity in tumor-associated macrophages to promote cancer growth and invasion. Genes Dev. 2010;24(3):241-55.
38. Galluzzi L, Kroemer G. Necroptosis: a specialized pathway of programmed necrosis. Cell. 2008;135(7):1161-3.
39. Aktipis CA, Boddy AM, Gatenby RA, Brown JS, Maley CC. Life history trade-offs in cancer evolution. Nat Rev Cancer. 2013;13(12):883-92.
40. Liu TT, Achrol AS, Mitchell LA, Rodriguez SA, Feroze A, Michael I, et al. Magnetic resonance perfusion image features uncover an angiogenic subgroup of glioblastoma patients with poor survival and better response to antiangiogenic treatment. Neuro Oncol. 2016.
41. Hu YL, DeLay M, Jahangiri A, Molinaro AM, Rose SD, Carbonell WS, et al. Hypoxia-Induced Autophagy Promotes Tumor Cell Survival and Adaptation to Antiangiogenic Treatment in Glioblastoma. Cancer Res. 2012;72(7):1773-83.
42. Hambardzumyan D, Bergers G. Glioblastoma: Defining Tumor Niches. Trends Cancer. 2015;1(4):252-65.